Research Paper
Carbon Reports
Vol. 2 No. 2 2023 91-96

Analysis of the intermediate states of an electrode slurry by electronic conductivity measurements

Mitsuhiro Takeno[a),b),c)], Seiji Katakura[c)], Kohei Miyazaki[a)], Takeshi Abe[a)] and Tomokazu Fukutsuka[c),*]

a) Graduate School of Engineering, Kyoto University: Kyotodaigakukatsura, Nishikyo-ku, Kyoto, Kyoto 615–8510, Japan
b) Research and Development Center, Panasonic Energy Co., Ltd.: 1–1 Matsushita-cho, Moriguchi, Osaka 570–8511, Japan
c) Graduate School of Engineering, Nagoya University: Furo-cho, Chikusa-ku, Nagoya, Aichi 464–8603, Japan

The electronic resistance of composite electrodes for lithium-ion batteries has a non-negligible effect on the charge–discharge performance at high rates. In order to obtain an electrode with a high-rate performance it is important that conductive materials, such as acetylene black (AB), in the electrode slurry form a good electron conduction network. This study evaluated the electron conduction network of various electrode slurries made using different processes and with different solid contents using electronic conductivity measurements of the electrode slurries. The conductivity of the slurry showed a correlation with the rate performance. Depending on the production method and solid content, the conductivity of the slurry changed. The results suggest that the electron conduction network of the slurry is modified by collisions between the AB and active material particles during kneading and by stirring the slurry with excess solvent during dispersion. Measuring the conductivity of the slurry is expected to help determine the conditions of its manufacture.

KEYWORDS : Lithium-ion batteries, Electrode slurry, Acetylene black, Mixing process

1. Introduction

More than 30 years have passed since lithium-ion batteries (LIBs) were commercialized, and their application has spread from mobile to large devices, such as stationary power supplies and electric vehicles (EVs) [1]. In these large devices, the demands on LIBs include high performance and low cost. From the viewpoint of industrial production, a simple and efficient method to produce LIBs is required to decrease their cost. The electrode slurry used for the positive electrode in LIBs is a mixture of active electrode material powder, conductive material powder such as acetylene black (AB), polymeric binder, and solvent [2]. The electrode slurry is coated on a metal current collector and dried to form a composite electrode. The composite electrode in LIBs has a porous structure, in which the electrode/electrolyte interface spreads in three dimensions, and both electrons and ions are conducted in the composite electrode. The reduction of internal resistance is indispensable for the use of LIB in EVs, where high-rate performance is required. The internal resistance includes both electronic resistance and ionic resistance as the components. The active electrode materials presently used in LIBs are not electronic conductors but semiconductors or insulators [3]. Therefore, adding ABs is indispensable, enabling electron conduction inside the composite electrode and reducing electronic resistance. The ionic resistance is composed of interfacial lithium-ion transfer resistance [4–7], lithium-ion diffusion resistance within the active material [3, 8–11], and ion transport resistance within the electrolyte and composite electrode [12–14]. Thus far, ionic resistance has been studied as the main component of internal resistance [15–17]. However, it has been reported that the influence of electronic resistance cannot be ignored at high rates [18–21].

This study focused on the electronic resistance of the composite electrode and developed a new method to measure the electronic conductivity of the electrode slurry. It was found that the network structure of the conductive material in the electrode slurry is important for the reduction of internal resistance [22–25]. Furthermore, the electronic resistance of the composite electrode is reduced by selecting the appropriate conductive material and mixing process [25]. This study demonstrated that AB acts as an effective conductive material and that the mixing process of AB and the active material in a low-viscosity state leads to a good electron conduction network structure in the electrode slurry. The electrode slurry mixed in the low-viscosity state finally becomes a high-viscosity state, which means that a relationship is found between the good electron conduction network structure in the electrode slurry and its high-viscosity. The viscosity of the

* Corresponding Author, E-mail: fukutsuka@nuee.nagoya-u.ac.jp
(Received November 30, 2022, Accepted February 15, 2023)
(J-STAGE Advance published February 24, 2023)

https://doi.org/10.7209/carbon.020201

electrode slurry affects the feeding and coating processes, which are important from the viewpoint of the industrial process. In the case of a high-viscosity electrode slurry, high transport energy is required to transport the electrode slurry from the tank, making it difficult to control the flow rate of the electrode slurry. Therefore, adding a solvent is necessary to decrease the viscosity of the electrode slurry. Unfortunately, the solvent needs to be removed during the drying process, which requires a large amount of heat. During the solvent removal, the electrode slurry reduces its uniformity, leading to a crack formation on the produced composite electrode. In addition, a low-viscosity electrode slurry gives a low electrode density, reducing the energy density of LIBs. Therefore, it is necessary to prepare an electrode slurry with a good electron conduction network structure with appropriate viscosity.

Rheological analysis is useful for investigating a dispersion system such as an electrode slurry; however, it is not a suitable technique for analyzing the electrode slurry at a high-viscosity state during the mixing process. In a concentrated system such as an electrode slurry, the interactions between the solvent and the solid particles largely depend on the concentration of the solid content; therefore, the rheological properties significantly change during the mixing process, causing difficulties of the detailed analysis. There are few methods for analyzing the electrode slurry during the mixing process, and there are no quantitative design guidelines for the electrode slurry mixing process that ensure good battery performance. This study investigates the electron conduction network in the electrode slurry during the mixing process by determining the electronic conductivity of the electrode slurries at the high-viscosity state.

2. Experimental

A solid-state method was used to synthesize $LiNi_{1/3}Mn_{1/3}Co_{1/3}O_2$ (NMC) particles from a mixture of Li_2CO_3 and $NiMnCo(OH)_2$ [26]. A mechanical stirrer (T.K. HIVIS MIX model 3D-5) was used to mix NMC particles with AB and polyvinylidene difluoride (PVdF) in 1-methyl-2-pyrrolidone (NMP). The electrode slurry has an NCM:AB:PVdF weight ratio of 90 : 6 : 4 wt%. The mixing processes 1–3 shown in **Fig. 1** were used to make slurries 1–3, respectively. After all the materials were injected, the electrode slurries were sampled every 30 min. To produce electrode slurries with different solid contents, NMP was added to slurries 1–3, and the solid content was reduced by 2% and 4% from those before the addition. After the addition, the mixture was stirred at 2500 rpm for 5 min using a T.K. ROBO MICS mixer.

The obtained electrode slurry was cast on a polyethylene terephthalate strip or aluminum foil to create a composite layer and a composite electrode, respectively. A scanning electron microscope (SEM) was used to observe the morphology of the composite electrode. The electronic volume resistivity of the composite layer was

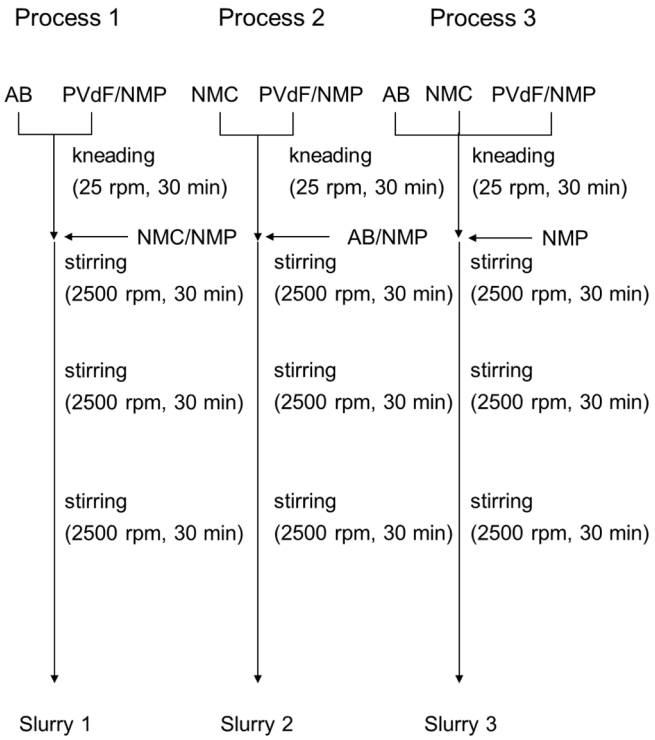

Fig. 1 Mixing processes used in the preparation of the electrode slurries.

measured by the four-point probe method using a Loresta IP MCP-250 apparatus. The electronic volume resistivity of the electrode slurry was measured by AC impedance spectroscopy utilizing a rheometer. A previous work shows the details [22]. The measurements of the steady-flow viscosity were performed on the electrode slurry at 25 °C with a strain-controlled rheometer.

A cell was assembled from a composite electrode (35 mm×35 mm), a negative electrode, an electrolyte of 1.5 mol dm^{-3} $LiPF_6$ dissolved in ethylene carbonate/ethyl methyl carbonate (1 : 3 by volume), and a microporous polyethylene separator. The state of charge of the cell was adjusted to 50%. An electrochemical apparatus (Solartron 1470E CellTest system) was used to perform galvanostatic polarization measurements. The cell was discharged at various currents for 10 s from the open circuit at 25 °C. The limiting discharge current rate (limiting rate) was determined to evaluate the rate performance. The limiting discharge current rate was defined as the maximum current that gave an open circuit voltage of >2.5 V after discharging for 10 s.

3. Results and Discussion

The amount of NMP added after kneading was selected to ensure that the viscosity of the electrode slurry was within the range of 2–3 Pa s, as measured by a B-type viscometer (TOKI. SANGYO). The solid content after kneading was 20% for process 1 and 73% for processes 2 and 3, respectively. **Table 1** presents the solid content and steady-flow viscosity of the prepared electrode slurry, the electronic volume resistivity of the composite layer (ρ_{ve}), electrode density after

pressing, and the limiting rate. The limiting rate was the lowest for process 3, in which the materials were added simultaneously. Process 1, in which AB and PVdF/NMP were kneaded together, followed by the addition of NMC/NMP, gave rise to the highest limiting rate. Since the composition of the composite electrode and the loading amount were the same for all the processes, this difference was due to the difference in the internal resistance. From a previous study, it is suggested that the kneading process, in which AB and the active material are mixed at the same time, needs high shear energy and destroys the electron conduction network structure, causing the increase of the electronic resistance of the composite electrode [25]. This is the case with process 3 in the present study, where AB and NMC initially coexisted. Therefore, it is reasonable to expect that the composite electrode from process 3 had higher electronic resistance than the others. However, no significant difference was found in ρ_{ve} values. It is possible that the AB concentration (6 wt%) exceeded the critical percolation concentration and was high enough to form sufficient electron conduction paths. Based on the electrode density after pressing, process 3 gave a smaller value, which means that the contact between ABs in the composite electrode would be weaker. Therefore, the electrode density after pressing might be related to the limiting rate in the bad case. **Fig. 2** shows the SEM images of the composite electrodes. NMC particles (white particles) were mainly observed for all processes. ABs (black parts) and NMC particles were visibly separated only for process 1, and the composite electrode was not uniform. Moreover, no significant difference was observed between processes 2 and 3, and the composite electrodes were uniform. The results above indicate that the difference in the limiting rate cannot be predicted only from ρ_{ve} values or SEM images of the composite electrode. Therefore, this study focused on the electrode slurry.

Table 1 Various properties of the electrode slurries.

	Slurry 1	Slurry 2	Slurry 3
Solid content/%	66	70	72
Viscosity/Pa s	2.2	2.6	2.4
ρ_{ve}/Ω cm	2.4	2.3	2.3
Electrode density after pressing/g cm^{-3}	2.66	2.66	2.63
Limiting rate/C	14.0	13.5	10.0

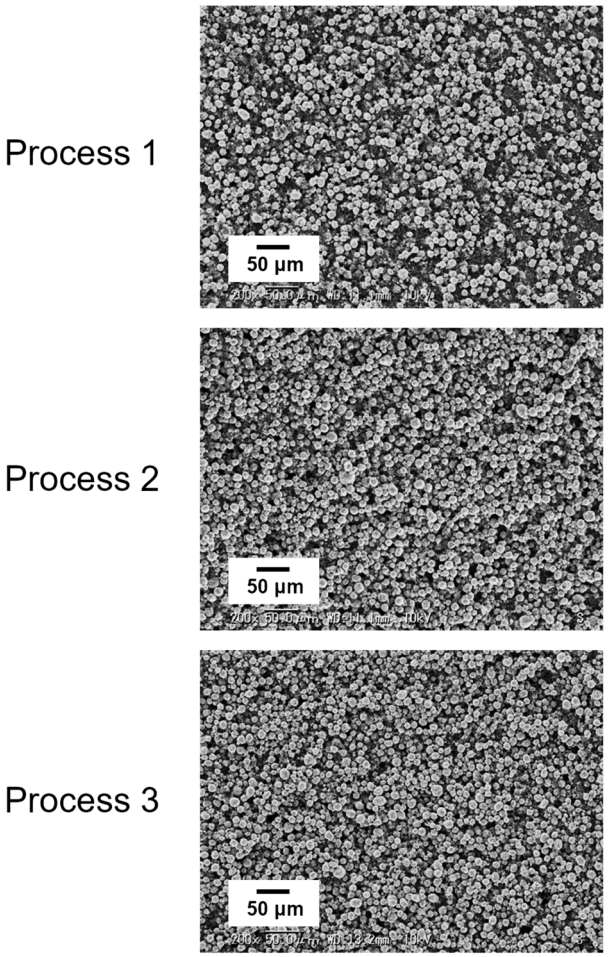

Fig. 2 SEM images of the composite electrodes.

Fig. 3 shows the steady-flow viscosity of the electrode slurries. The steady-flow viscosities followed the order of slurry 2> slurry 3> slurry 1. The lowest viscosity of slurry 1 is due to the smallest solid content. Despite the largest solid content, the viscosity of slurry 3 was lower than that of slurry 2, probably because the AB network structure grows weakly in slurry 3. **Fig. 4** shows the values of the electronic volume resistivity of the electrode slurries (ρ_{vs}) and ρ_{ve} at each sampling time (30, 60, and 90 min). The values of ρ_{vs} at 90 min followed the order of slurry 3> slurry 2> slurry 1, which agreed with the order of the limiting rates presented in **Table 1**. In other words, ρ_{vs} was found to be correlated with the limiting rate. In process 3, ρ_{vs} already reached a high value at 30 min but less increased at 60 min compared with those in processes 1 and 2, which almost had the same ρ_{vs} values at 60 min and 90 min. This is because the AB network structure was destroyed in the initial stage of the kneading

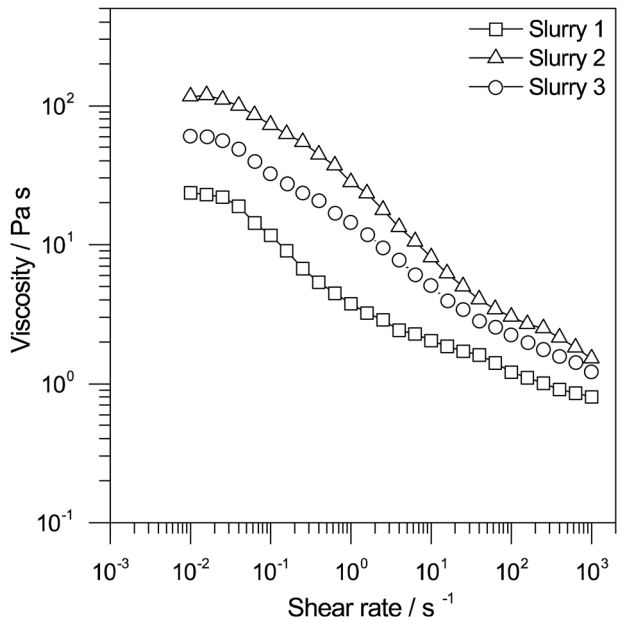

Fig. 3 Steady-flow viscosity of the electrode slurries.

process, where the AB and NMC were kneaded under coexistence. The ρ_{vs} values in processes 1 and 2 were low at 30 min and increased considerably by 60 min. The increases in ρ_{vs} values at 90 min from 60 min were larger for slurry 3 than that for slurry 2. The collisions of AB and NMC destroyed the AB network structure during stirring, and large agglomerates of AB were broken down into relatively small agglomerates. The destruction of the AB network structure eventually stopped, and the increase in ρ_{vs} became gradual. On the other hand, ρ_{ve} was not considerably different in each process and did not significantly depend on the stirring time. This is because the volume fraction of AB was large and sufficiently over the critical percolation concentration. The above results show that ρ_{vs} is strongly correlated with the limiting rate rather than ρ_{ve}, and the electronic conductivity measurement of the electrode slurry is a useful analytical method to detect changes in the microstructure of the AB network during the mixing process.

The solid content of the electrode slurry is important for the coating process, as mentioned in the introduction. Therefore, it is necessary to investigate the influence of the solid content on the electrode slurry in each process. **Fig. 5** shows the values of ρ_{vs} and the viscosity of the electrode slurries with various solid contents. The solid contents of 68% and 70% for slurry 3, 68% and 66% for slurry 2, and 64% and 62% for slurry 1 were achieved by adding NMP to slurries 1–3, while slurry 1 with a solid content of 68% was prepared by process 1 separately. For all the slurries, ρ_{vs} increased with a decrease in the solid content (an increase in the NMP content) because NMP is an insulator. The viscosity of the electrode slurries was also dependent on the solid content, although the changes were small. At the same solid content of 68%, the ρ_{vs} values were in the order of slurry 3> slurry 2> slurry 1. This indicated that the addition of NMP does not drastically change the AB network structure formed during the preparation process of the electrode slurry and that the reduction in the solid content increases the value of ρ_{vs} via the difference in the volume fraction. However, the slope of the ρ_{vs} plot had a different tendency for each electrode slurry. For slurry 3, the slope was gradual compared with slurries 1 and 2. Since the AB network structure of slurry 3 was destroyed on kneading, the influence of the reduction in solid content due to the addition of NMP was less than that for slurries 1 and 2. In other words, the AB network structures in slurries 1 and 2 were disturbed by stirring them with excess NMP. The above

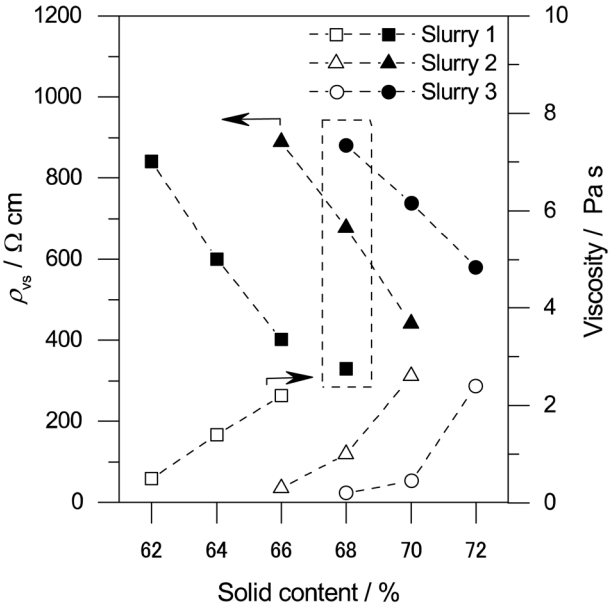

Fig. 5 Electronic volume resistivity and viscosity of the electrode slurries at various solid contents.

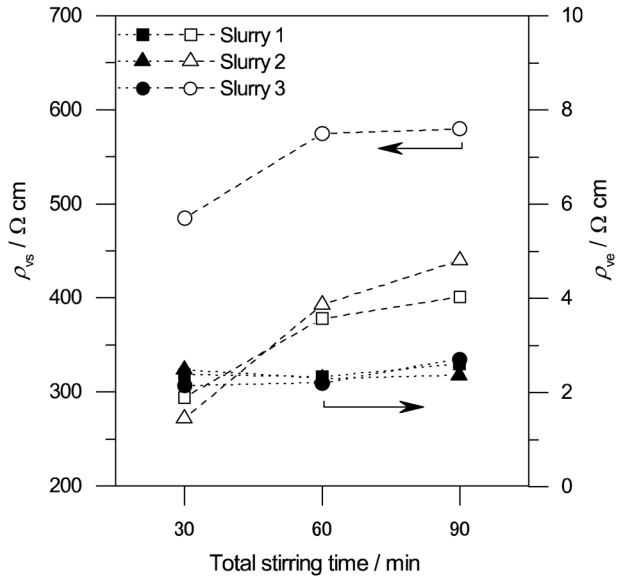

Fig. 4 Electronic volume resistivity of the electrode slurries (open symbols) and the composite sheets (closed symbols) as a function of the total stirring time.

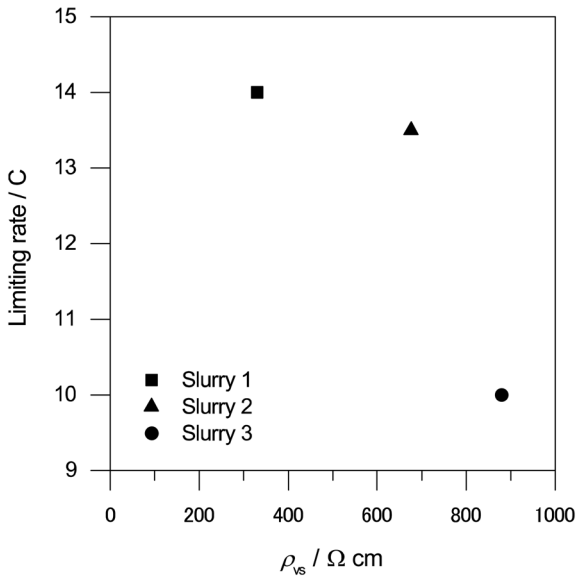

Fig. 6 Limiting discharge current rate for the electrode slurry with a solid content of 68% as a function of the electronic volume resistivity of the electrode slurry.

results show that the relationship between the microstructure of the network structure and the solid content, which cannot be determined by the rheological analysis, can be evaluated from the measurements of the electronic conductivity of the electrode slurry.

Finally, the limiting rates were examined for the composite electrodes produced from the electrode slurry with a solid content of 68%. **Fig. 6** shows a plot of the limiting rate against ρ_{vs}. Processes 1 and 2 gave a high limiting rate, while process 3 gave rise to a low limiting rate, which means that the limiting rate was correlated with ρ_{vs} for processes 1 and 3. However, a high limiting rate was observed for process 2 despite the high ρ_{vs} value. The AB network forms a bulky structure in the electrode slurry, and the microstructure is reflected in the composite electrode after coating and drying. As a result, the produced composite electrode can have different porous structures even with the same solid content. In the case of process 2, it is likely that ion conduction strongly influences the internal resistance rather than electron conduction.

4. Conclusion

This study investigated the intermediate states of the electrode slurry during the preparation process via electronic conductivity measurements. Changes in the AB network structure were clarified by investigating the temporal changes in the electronic conductivity of the electrode slurry during the mixing process. It was found that the electronic volume resistivity of the electrode slurry was dependent on the solid content. However, it was revealed that even if at the same solid content of the electrode slurry, the electronic volume resistivity of the electrode slurry varied, which also affected the limiting current. It is possible to predict the electronic resistance of the electrode slurry at arbitrarily defined solid content by determining the correlation between the solid content and the electronic volume resistivity of the electrode slurry in advance. As a result, the preparation conditions of the electrode slurry, such as the solid content and viscosity, can be decided in detail.

Acknowledgements

This work was partially supported by CREST, JST (JPMJCR12C1).

References

[1] M. Armand, J.M. Tarascon, Building better batteries, Nature 451 (2008) 652–657.

[2] J.L. Li, C. Daniel, D. Wood, Materials processing for lithium-ion batteries, J. Power Sources 196 (2011) 2452–2460.

[3] M. Park, X.C. Zhang, M.D. Chung, G.B. Less, A.M. Sastry, A review of conduction phenomena in Li-ion batteries, J. Power Sources 195 (2010) 7904–7929.

[4] I. Yamada, T. Abe, Y. Iriyama, Z. Ogumi, Lithium-ion transfer at $LiMn_2O_4$ thin film electrode prepared by pulsed laser deposition, Electrochem. Commun. 5 (2003) 502–505.

[5] T. Abe, H. Fukuda, Y. Iriyama, Z. Ogumi, Solvated Li-Ion Transfer at Interface Between Graphite and Electrolyte, J. Electrochem. Soc. 151 (2004) A1120.

[6] T. Abe, M. Ohtsuka, F. Sagane, Y. Iriyama, Z. Ogumi, Lithium Ion Transfer at the Interface between Lithium-Ion-Conductive Solid Crystalline Electrolyte and Polymer Electrolyte, J. Electrochem. Soc. 151 (2004) A1950.

[7] T. Abe, F. Sagane, M. Ohtsuka, Y. Iriyama, Z. Ogumi, Lithium-Ion Transfer at the Interface Between Lithium-Ion Conductive Ceramic Electrolyte and Liquid Electrolyte-A Key to Enhancing the Rate Capability of Lithium-Ion Batteries, J. Electrochem. Soc. 152 (2005) A2151.

[8] K. Dokko, M. Mohamedi, Y. Fujita, T. Itoh, M. Nishizawa, M. Umeda, I. Uchida, Kinetic Characterization of Single Particles of $LiCoO_2$ by AC Impedance and Potential Step Methods, J. Electrochem. Soc. 148 (2001) A422.

[9] M.D. Levi, G. Salitra, B. Markovsky, H. Teller, D. Aurbach, U. Heider, L. Heider, Solid-State Electrochemical Kinetics of Li-Ion Intercalation into Li_{1-x} CoO_2: Simultaneous Application of Electroanalytical Techniques SSCV, PITT, and EIS, J. Electrochem. Soc. 146 (1999) 1279–1289.

[10] J. Marzec, K. Świerczek, J. Przewoźnik, J. Molenda, D.R. Simon, E.M. Kelder, J. Schoonman, Conduction mechanism in operating a $LiMn_2O_4$ cathode, Solid State Ion. 146 (2002) 225–237.

[11] M.D. Levi, D. Aurbach, Diffusion Coefficients of Lithium Ions during Intercalation into Graphite Derived from the Simultaneous Measurements and Modeling of Electrochemical Impedance and Potentiostatic Intermittent Titration Characteristics of Thin Graphite Electrodes, J. Phys. Chem. B 101 (1997) 4641–4647.

[12] T. Fukutsuka, K. Koyamada, S. Maruyama, K. Miyazaki, T. Abe, Ion Transport in Organic Electrolyte Solution through the Pore Channels of Anodic Nanoporous Alumina Membranes, Electrochim. Acta 199 (2016) 380–387.

[13] Y.H. Chen, C.W. Wang, X. Zhang, A.M. Sastry, Porous cathode optimization for lithium cells: Ionic and electronic conductivity, capacity, and selection of materials, J. Power Sources 195 (2010) 2851–2862.

[14] C. Fongy, S. Jouanneau, D. Guyomard, J.C. Badot, B. Lestriez, Electronic and Ionic Wirings Versus the Insertion Reaction Contributions to the Polarization in $LiFePO_4$ Composite Electrodes, J. Electrochem. Soc. 157 (2010) A1347.

[15] Y. Orikasa, Y. Gogyo, H. Yamashige, M. Katayama, K. Chen, T. Mori, K. Yamamoto, T. Masese, Y. Inada, T. Ohta, Z. Siroma, S. Kato, H. Kinoshita, H. Arai, Z. Ogumi, Y. Uchimoto, Ionic Conduction in Lithium Ion Battery Composite Electrode Governs Cross-sectional Reaction Distribution, Sci. Rep. 6 (2016) 26382.

[16] G. Inoue, M. Kawase, Numerical and experimental evaluation of the relationship between porous electrode structure and effective conductivity of ions and electrons in lithium-ion batteries, J. Power Sources 342 (2017) 476–488.

[17] D. Guy, B. Lestriez, R. Bouchet, D. Guyomard, Critical Role of Polymeric Binders on the Electronic Transport Properties of Composites Electrode, J. Electrochem. Soc. 153 (2006) A679.

[18] Z.L. Liu, J.Y. Lee, H.J. Lindner, Effects of conducting carbon on the electrochemical performance of $LiCoO_2$ and $LiMn_2O_4$ cathodes, J. Power Sources 97–98 (2001) 361–365.

[19] S. Mandal, J.M. Amarilla, J. Ibáñez, J.M. Rojo, The Role of Carbon Black in $LiMn_2O_4$-Based Composites as Cathodes for Rechargeable Lithium Batteries, J. Electrochem. Soc. 148 (2001) A24.

[20] Z.H. Chen, J.R. Dahn, Reducing Carbon in $LiFePO_4$ /C Composite Electrodes to Maximize Specific Energy, Volumetric Energy, and Tap Density, J. Electrochem. Soc. 149 (2002) A1184.

[21] H.Y. Tran, G. Greco, C. Täubert, M. Wohlfahrt-Mehrens, W. Haselrieder, A. Kwade, Influence of electrode preparation on the electrochemical performance of $LiNi_{0.8}Co_{0.15}Al_{0.05}O_2$ composite electrodes for lithium-ion batteries, J. Power Sources 210 (2012) 276–285.

[22] M. Takeno, T. Fukutsuka, K. Miyazaki, T. Abe, Development of New Electronic Conductivity Measurement Method for Lithium-ion Battery Electrode–Slurry, Chem. Lett. 46 (2017) 892–894.

[23] M. Takeno, T. Fukutsuka, K. Miyazaki, T. Abe, Influence of carbonaceous materials on electronic conduction in electrode-slurry, Carbon 122 (2017) 202–206.

[24] M. Takeno, T. Fukutsuka, K. Miyazaki, T. Abe, Investigation of Electronic Resistance in Lithium-Ion Batteries by AC Impedance Spectroscopy, J. Electrochem. Soc. 164 (2017) A3862–A3867.

[25] M. Takeno, S. Katakura, K. Miyazaki, T. Abe, T. Fukutsuka, Relation between Mixing Processes and Properties of Lithium-ion Battery Electrode-slurry, Electrochemistry 89 (2021) 585–589.

[26] T. Ohzuku, Y. Makimura, Layered Lithium Insertion Material of $LiCo_{1/3}Ni_{1/3}Mn_{1/3}O_2$ for Lithium-Ion Batteries, Chem. Lett. 30 (2001) 642–643.